IECMS 2020

sciforum

Conference Proceedings Paper

The exploration of metallic deposits using satellite image processing in the Parwan-Panjshir area, Afghanistan

Mahdi Khalaj [1], Ziba Karimi [2] and Mohsen Rabbani[2]

1 Mining Department; Omran Mining and Geotechnic Company (OMG/OGC), Miningdepartment@ogc.af
2 Ministry of Mines and Petroleum; Zibakarimi513@gmail.com

* Correspondence: Mining@ogc.af; Tel.: +93-702-360-037

Received: date; Accepted: date; Published: date

Abstract: The unique tectonic features have resulted in diverse metallic and non-metallic mineralization in Afghanistan. Hence, this paper focused on the development of exploration and mineral resources data in Afghanistan. The study area is located in the western Hindu Kush tract and on the northern verge of the Hari-Rod-Panjshir fault, Afghanistan, that mainly associates with the western Hindu Kush and Badakhshan plutonic belts. The rock units include crystalline limestones and diabase formed during the Paleozoic era and Triassic period. The aim of this study was to employ Remote Sensing (RS) methods by using the Landsat-8 satellite and ASTER sensor to spot iron and copper mineralization zones in the Parwan-Panjshir area. Therefore, Band Composition, Principal Component Analysis (PCA), and Band Ratio were applied to identification of iron oxide minerals. The detected area provided by satellite images had very good compliance with the results of field studies. Furthermore, mineralization of carbonate host-rocks iron and Fe–Cu–(Au) skarn were observed during field surveys. Hematite–Magnetite, Chalcopyrite, and pyrite mineralization have resulted from the injection of various diabase subvolcanic into carbonate units. Also, high heat flow has caused widespread marble formation in the area. The results were supported by microscopic and geochemical studies.

Keywords: Afghanistan; Parwan-Panjshir; Fe-Cu-(Au) skarn; Remote Sensing; Exploration; Principal Component Analysis (PCA)

1. Introduction

mineralization process in Afghanistan comprises a wide range of metallic and non-metallic deposits with a high level of value, volume, and grade [1, 2]. Although there are a wide range of mineral resources in Afghanistan, almost all of these mineral deposits have not been systematically explored or successfully mined [3]. There are many techniques for mineral exploration in which two common techniques are Remote Sensing (RS) images and field studies [4]. In general, RS is an effective tool to collect raster data and images, a rapid technique to detect distinctive adsorption features of hydrothermal alteration ore minerals, and a reliable method to provide geological mapping [5].

After defining the problems, the purpose of this study was explained to develop geological exploration information about iron mineralization in Afghanistan by employing RS technique and Field Survey. Therefore, an accessible study area locating on the northern verge of Hari-Rod-Panjshir fault was selected because this AOI is the largest iron ore deposit in centra iron belt of Afghanistan (Haji Gak-Panjshir-Badakhshan iron belt) [6]. To characterize geological data about this unstudied area, available data derived from previous studies about Parwan-Panjshir AOI were collected and the distribution of iron oxide was identified by processing of Landsat and ASTER Images [7-9]. Additionally, to confirm results, field survey and rock sampling were performed and XRF analyses, determination of the grade of elements, and studies of polished sections were carried out on some collected samples from AOI.

1.2. Regional geology

Afghanistan has complex geology with rocks revealing every geologic age from Archean to the present. In other words, there is a comprehensive of varied crustal blocks separated by major fault zones in which each block is characterized by a different history and metallogenic feature. The occurrences and iron deposits are present in the Hari-Rod-Panjshir Zone (the central part Afghanistan) and along 600 km from east to west. The host rock types related to these AOI are Proterozoic metamorphic carbonate and volcanic rocks. Many of the iron deposits and the occurrences are hematite-magnetite such as Haji Gak iron ore deposit, the largest hematite-magnetite deposit in the Middle East [10] (Figure 1-a).

The Middle Paleozoic metamorphic rocks showed by a Silurian-Lower Carboniferous marble and Lower Carboniferous and Upper Carboniferous-Lower Permian terrigenous schist are the main geological characteristic of the Panjshir Valley and around it.

The AOI consists of fragmented structures and various fault blocks and its largest area mainly includes mélange zones, which is on the verge of main faults, with composition of carbonate rocks, tuffs, basaltic units, siliceous rocks and small granitic apophyses (Figure 1-b).

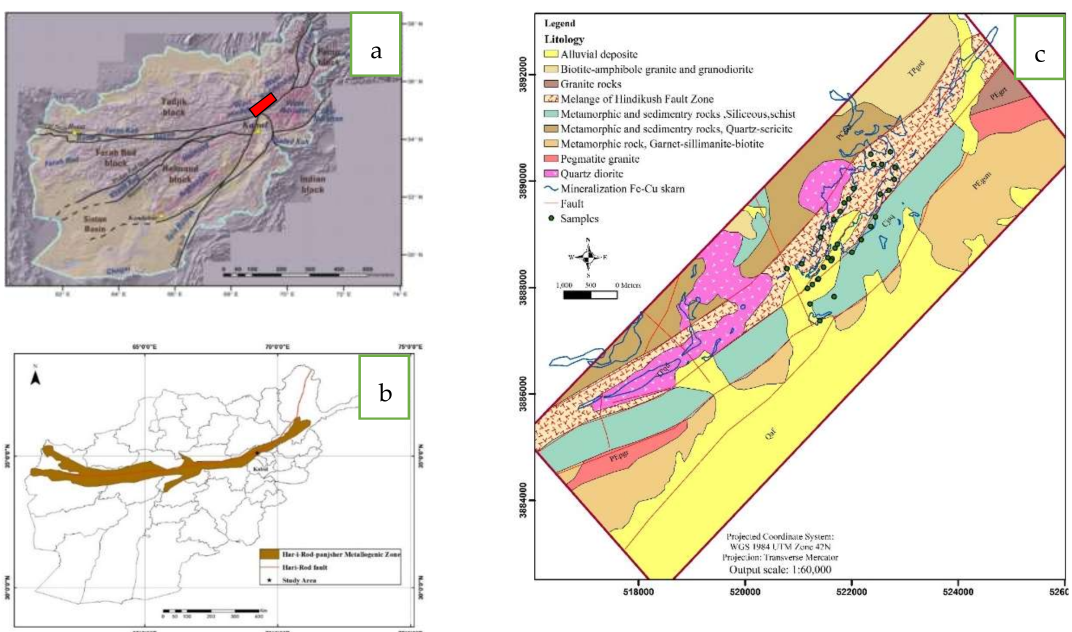

Figure 1 a: Map of Afghanistan. Corresponding colors for major structural blocks, plutonic belts and faults are dark brown labels, blue labels, and black labels, respectively. Plutonic rocks are represented in red, other around rocks in beige, and unconsolidated Quaternary sediment in yellow. (the area of interest is in red). **b**: Area pertinent to iron and Skarn mineralization along with some of main faults are determinate on the map. Geologic and Mineral Map of AOI (prepared by USGS). c: It should be noted that the scale of USGS map is 1:100,00 and this map was prepared by using old information (1975) and satellite images, therefore, it would not be very accurate because there are some differences between field surveys' result and this map (host-rocks for iron-copper mineralization are carbonate rocks [11].

2.Material and methods

2.1.Remote Sensing

Obviously, RS tool plays an important role in identification and distinction of altered zones and associated intrusions and hydrothermal fluids. In addition, due to multi-spectral and covering vast areas and mineralization zones associated with altered zones, satellite images widely have been used [12]. In this study, firstly, iron oxide and clay minerals occurrence in Panjshir iron deposits were detected by using Band Ratio (BR) and Principal Components Analysis (PCA) techniques. Furthermore, results derived from satellite image processing techniques for iron oxide map preparation were investigated based on obtained data from field survey, petrographic study of polished sections, and geochemical analyses [13].

A False Color Composite (FCC) is an image processing technique that has appropriate results is a common method to generate colorful images by using three different Bands 7 (in red), 5 (in green) and 2 (in blue). Since Landsat 8 has more bands in the visible range and the ASTER has more bands in the short infrared range, their color combination can be used to identify iron oxide and hydroxide group minerals and alterations, respectively. The RGB color composite of OLI bands 651 sensors (figure 2-a) is an effective tool for identifying iron oxides and hydroxides. As can be seen, areas with iron oxides and hydroxides are displayed in red and orange colors, clay alterations and phyllite in beige.

OLI data possesses a great capability for lithological mapping. A false color composite image of Bands 7 (in red), 5 (in green) and 2 (in blue) is generated. By comparison of very high values for iron oxide-bearing areas.

The Band Ratio is one of the spectral techniques that ratios are simply the divide one band by another band to create a spectral index. Band Ratios is used to enhance the spectral differences between bands and to reduce the effects of topography. Dividing one spectral band by another produces an image that provides relative band intensities. The Band Ratio image enhances the spectral differences between bands and can be useful when trying to discriminate between land cover types. For this reason, in this study, ASTER sensor images were used [14].

Since high values in band ratio 4/2 is sensitive to low concentration of ferric iron, this band is very effective not only to identify the the charge transfer absorption of ferric iron oxides in the blue spectral region but also to highlight iron oxides of mafic regolith [15]. The white pixels in Figure 2-b displays the ferric iron occerrence in the AOI.

PCA, which is mostly used in the earth science, is technique to maximize showing of the differences between spectral bands and compacting resulted data as a new linear recombination of features to generate separate and independent bands [16]. In this work, PCA was utilized to highlight iron oxide zones. In this regard, Band 6 had the best compatibility with iron oxide among other designed Bands (2, 3, 4, 5, and 7). In Figure 2-c, the white pixels showing iron oxide-bearing zones.

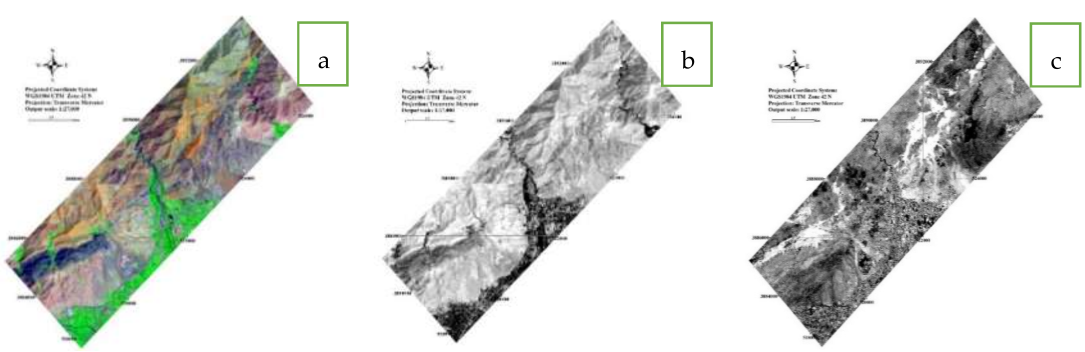

Figure 2: **a**: Geological map resulted from color composition R:7, G:5, and B:2. The iron-bearing zones are marked with orange color. **b**: the band ratio of 4/2 used on ASTER sensor images shows iron oxide zones as white pixels, **c**: PCA on Band 6 of ASTER sensor well displaying iron as white pixels.

2.2.Mineralization

The Panjshir Valley emerald, iron, and silver AOI lies within the Hari Rud-Panjshir Metallogenic Zone, which extends through the whole Afghanistan from the western frontier eastward, is consist of a variety of mineral occurrence types and commodities, including barite, emerald, gold, iron, lead, manganese, mercury, silver, sulfur, and zinc. [17]

According to geological evidence, geochemical studies, and polished sections studies, there is a possibility of forming two types of mineralization in this AOI including: a hematite-magnetite mineralization and Cu-skarnization with minor amount of Au. The former one was formed in the form of different size lenses within carbonate units and simultaneously with sedimentation (Figure 3-a). These units contain silver and iron content of these lenses is high (up to 65% of weight of iron). These lenses mainly follow the stratification of their Protozoic host-rock (up to 70 degrees to the northwest). Cu-skarnization with Au was created by lying basaltic-diabase lavas into carbonate units containing iron lenses, (Figure 3-b and 3-c), that resulted in generation of heat flow and the crystallization of carbonate (marble) units and the mobilization of iron are relative to its previous formation zone. For this reason, the high and low level of Fe-skarnization in different zones is explicable. Also, these two types of mineralization are confirmed by less mobility of iron occurrence in crystalline carbonate lenses units and no copper mineralization (chalcopyrite) occurrence, which are far from basalt-diabase occurrence. The skarnization system, as the main purpose of this work, will be explained in follows.

Injection of basalt-diabase into carbonate rocks has caused isochemical metamorphism of the intrusive rocks and the formation of marble and hornfels. Crystallization during the cooling of magmatic flow has caused the evolution of the hydrothermal fluid phase and its penetration into carbonate entrapment rocks. The reaction of these fluids with primary metamorphic rocks caused extensive metasomatic metamorphism by the formation of anhydrous calc silicate minerals (pyroxene) and then hydrated calc silicate minerals (epidote and thermolite-actinolite), silicate (quartz), clay (chloride), oxidized (magnetite-hematite), sulfide (pyrite and chalcopyrite), and carbonate (calcite) (Figure 3-d). In addition, in the contact of basalt-diabase units with carbonate rocks, hornfels is characterized by dense texture, intense silicification, the presence of high temperature minerals such as pyroxene, as well as chalcopyrite, magnetite, and pyrite mineralization.

Due to the oxidation conditions prevailing in the region occurred after the formation of mineralization, magnetite has been converted to hematite, major copper sulfide ores to azurite, and finally pyrite to oxide and iron hydroxides. Due to the formation of acidic solutions in the presence of atmospheric fluids, pyrite ore has intensified leaching and weathering in the ore-bearing areas.

The petrography study of 4 polished sections of iron lenses and skarn zones was carried out to understand the nature of mineralization as well as to study the relationships between minerals. The geological and geochemical data were confirmed by the results of these studies confirmed. The corresponding mineral types for skarnization of chalcopyrite, pyrite, and magnetite ores and chalcocite, azurite, malachite, hematite, and other iron oxides ores are primitive and secondary, respectively (Figure 3-e).

Furthermore, petrography of polished sections of collected samples of iron lenses from AOI indicated the presence of hematite minerals along with primary pyrite voids, which is destroyed under the leaching process (Figure 3-f).

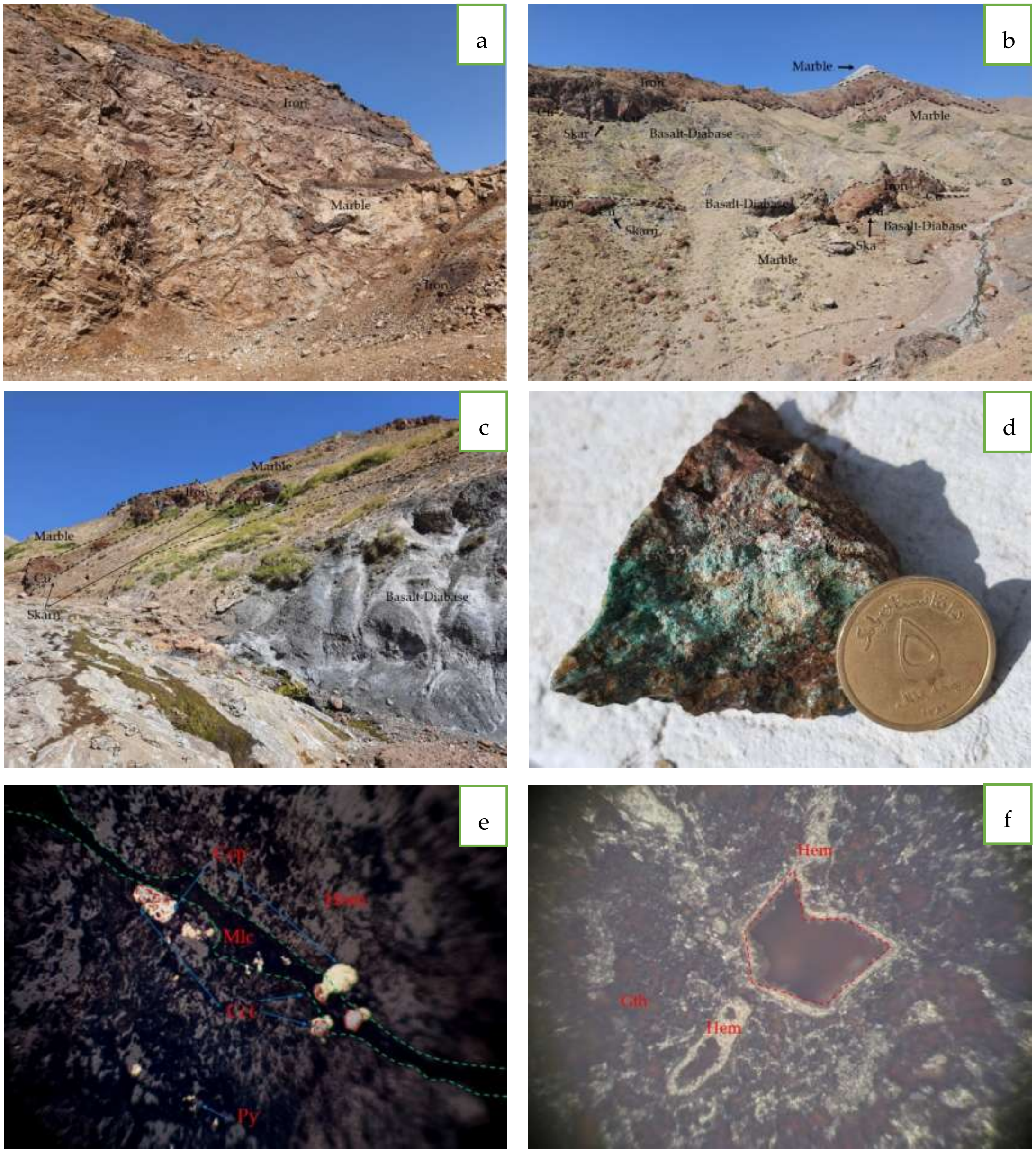

Figure 3, **a**: The presence of hematite lenses inside the crystallized carbonate host-rock. **b** and **c**: In this image, iron lenses of different sizes are shown. Also, the conformable of basaltic-diabase units with ferrous carbonate units has caused copper-gold skarsification and mineralization. **d**: A collected sample from skarn zone by the presence of malachite, quartz, calcite, pyroxene, and hematite. **e**: Prepared polishing section from skarn zone in which the presence of chalcopyrite (Ccp) and pyrite (Py) ores (as primary ores) and malachite (Mlc), chalcocite (Cct), and hematite (Hem) are present. **f**: This image belongs to the polishing section of iron ore in lenses enclosed in crystalline carbonate units. Hematite iron (Hem) with goethite (Gth) containing voids left from primary pyrite.

2.3.Geochemistry

To analyze elements in the basic and skarn units, 30 sample were collected from skarn and iron lenses in the carbonate host-rocks and basalt-diabase units. The samples were analyzed by a handheld XRF (Niton XL3t GOLDD+). Due to the large number of XRF analyzes and its comparison with ICP-MS analysis data, the accuracy of the obtained data is confirmed by a factor of 90% and some results obtained mentioned as follows:

- Silver in lenses containing iron is higher than the skarn zone. The correlation of Fe with Ag in iron lenses is above 0.9.

- According to the correlation (Table 1), there is no positive correlation between the elements of samples collected from iron and skarn mineralization and there is no good correlation between Fe and Cu. The corresponding correlation between Fe and Cu for samples collected from skarn and iron lenses are 0.4 and -0.25, respectively (Table 1).

- According to the diagrams using to differentiate the types of iron deposits and also the basis of this classification is the chemical analysis of magnetite and hematite types of iron oxide deposits, collected samples from the skarn zone are in the skarn range [18] (Figure 4).

a

	Ba	Sn	Ag	Mo	Nb	Sr	As	Pb	W	Zn	Cu	Ni	Fe	Mn	Cr	V	Ca	K	Al	Si	Cl	S
Ba	1																					
Sn	0.755048	1																				
Ag	0.908697	0.793284	1																			
Mo	0.972387	0.617612	0.875597	1																		
Nb	0.852117	0.408479	0.705076	0.921093	1																	
Sr	0.970552	0.751977	0.910472	0.953264	0.7907	1																
As	-0.9084	-0.75087	-0.88083	-0.91542	-0.82575	-0.91529	1															
Pb	-0.79661	-0.69574	-0.80893	-0.82516	-0.76211	-0.82872	0.97036	1														
W	0.852042	0.549362	0.821701	0.89132	0.734541	0.887185	-0.79498	-0.6942	1													
Zn	0.179502	-0.09095	-0.03078	0.191842	0.178272	0.224097	-0.10671	-0.05459	0.05377	1												
Cu	-0.17831	0.035696	-0.07188	-0.25584	-0.16419	-0.27242	0.180482	0.188157	-0.2885	-0.56929	1											
Ni	0.260677	0.226436	0.152805	0.256839	0.364765	0.22172	-0.32994	-0.40763	-0.14412	0.438613	-0.22177	1										
Fe	0.98277	0.754367	0.902245	0.967442	0.852701	0.972629	-0.94348	-0.86163	0.827711	0.263222	-0.25771	0.373881	1									
Mn	0.96144	0.729606	0.894602	0.955386	0.84468	0.971335	-0.9359	-0.87251	0.81361	0.297948	-0.27596	0.408279	0.991057	1								
Cr	0.926836	0.740048	0.8184	0.851448	0.718496	0.895995	-0.77638	-0.6534	0.659592	0.388622	-0.13954	0.416632	0.921787	0.913996	1							
V	0.629789	0.366866	0.633068	0.678467	0.753611	0.58515	-0.70979	-0.70973	0.436161	0.298414	-0.36055	0.571801	0.699921	0.70453	0.572424	1						
Ca	-0.98991	-0.73068	-0.89331	-0.97153	-0.87032	-0.974	0.93094	0.832558	-0.83733	-0.24149	0.190064	-0.29188	-0.98541	-0.97482	-0.92271	-0.66587	1					
K	0.453944	0.470433	0.513041	0.407265	0.353004	0.353508	-0.32281	-0.28499	0.30397	-0.44104	0.288328	0.113293	0.384639	0.38295	0.396038	0.159341	-0.38969	1				
Al	0.733057	0.714996	0.744013	0.621573	0.410709	0.740211	-0.64115	-0.50594	0.592424	0.363928	0.007879	0.066069	0.72916	0.718596	0.824157	0.379257	-0.74564	0.175376	1			
Si	-0.62278	-0.59356	-0.64638	-0.66322	-0.57631	-0.7387	0.802523	0.875807	-0.62368	-0.1696	0.456273	-0.394	-0.72135	-0.76817	-0.50555	-0.60121	0.668187	-0.10266	-0.35941	1		
Cl	0.788679	0.57468	0.758099	0.814679	0.772433	0.715559	-0.73602	-0.69438	0.68985	-0.27169	-0.03829	0.240994	0.753384	0.7321	0.608978	0.505216	-0.74072	0.777322	0.262917	-0.49203	1	
S	-0.70017	-0.47178	-0.69695	-0.7647	-0.77061	-0.66778	0.815074	0.84299	-0.5593	-0.04527	0.206328	-0.46686	-0.74724	-0.76718	-0.56217	-0.75416	0.727002	-0.54898	-0.32453	0.66095	-0.79378	1

b

	Ba	Sr	Rb	As	Pb	W	Zn	Cu	Ni	Fe	Mn	Cr	V	Ti	Ca	K	Al	Si	Cl	S
Ba	1																			
Sr	0.883044	1																		
Rb	0.640375	0.672885	1																	
As	0.159392	-0.09525	-0.36413	1																
Pb	0.65645	0.51903	0.36792	0.522072	1															
W	0.394774	0.214026	-0.02476	0.479698	0.431081	1														
Zn	-0.52743	-0.51722	-0.53205	0.193178	-0.1125	-0.26202	1													
Cu	0.416607	0.120511	0.116229	0.019514	0.19532	0.597389	-0.37206	1												
Ni	-0.37397	-0.45156	-0.6047	0.331081	-0.33664	-0.12989	0.638872	-0.09566	1											
Fe	0.092039	-0.04853	-0.4156	0.408633	-0.12433	0.521778	-0.1385	0.403226	0.355515	1										
Mn	-0.12011	-0.24978	-0.64364	0.229452	-0.18536	0.194727	0.360657	0.408894	0.661373	0.670448	1									
Cr	0.023444	0.003755	0.316213	0.170746	0.337513	0.125753	0.237993	-0.26813	-0.31339	-0.18151	-0.43908	1								
V	0.256953	0.449426	-0.12496	0.068113	0.078953	-0.05337	-0.08273	-0.23908	0.145382	-0.00387	0.187816	-0.56213	1							
Ti	-0.05218	0.057058	0.139443	-0.40199	0.04435	0.263299	-0.21201	0.258146	-0.55839	-0.26174	-0.11024	0.048662	0.035558	1						
Ca	0.820995	0.825557	0.582827	-0.02491	0.463748	0.437863	-0.77043	0.352534	-0.68999	0.211459	-0.23227	0.096084	0.160803	0.227812	1					
K	0.599025	0.619269	0.80018	-0.28772	0.424892	0.248054	-0.45367	0.320275	-0.64085	-0.03906	-0.30911	0.482882	-0.27529	0.336302	0.716092	1				
Al	0.512638	0.50174	0.201513	-0.17258	-0.08174	0.242312	-0.09085	0.37483	0.149569	0.490472	0.446175	-0.07246	0.168843	-0.10456	0.42269	0.403385	1			
Si	0.365891	0.487996	0.107156	0.157137	0.13497	0.217111	-0.11332	-0.012	0.140995	0.542478	0.34507	0.079749	0.351867	-0.06465	0.433487	0.391345	0.613268	1		
Cl	-0.25165	-0.35745	0.049665	-0.48521	-0.61025	-0.33788	-0.01148	0.222345	0.236156	-0.17904	-0.01593	-0.36707	-0.31071	-0.19291	-0.40303	-0.26114	0.043376	-0.57572	1	
S	-0.20524	-0.39905	-0.18925	0.126843	0.040687	0.05859	0.087012	0.125963	-0.07891	-0.30788	-0.25209	-0.05659	-0.34353	-0.09655	-0.31284	-0.41375	-0.52409	-0.92355	0.451261	1

Table 1, **a**: Correlation table between elements in iron ore (Parwan-Panjshir AOI), which exists as lenses in crystallized carbonate rocks. As can be seen, there is a high correlation between Fe and Ba, Sn, Ag, Mo, Nb, Sr and W. **b**: Correlation of elements in Skarn zone samples, which only shows the positive correlation between Cu and W. In both graphs there is no proper correlation between Fe and Cu.

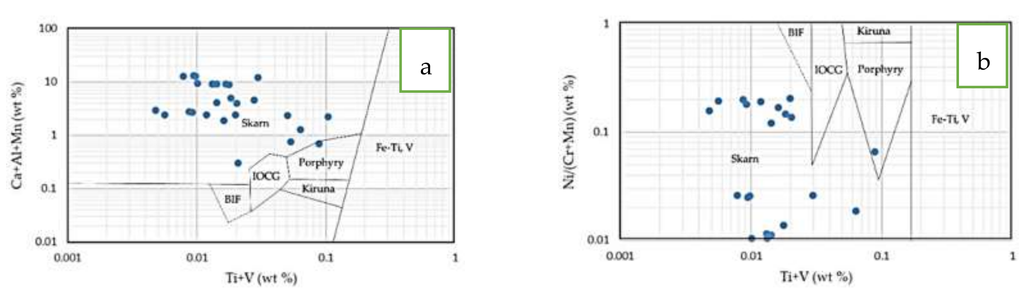

Figure 4, Location of iron-containing samples in the skarn zone of Parwan-Panjshir AOI. In both diagrams, the samples are in the skarn section.

3.Conclusion

-Using Remote Sensing processes on ASTER and ETM8 sensors, the best performance in this area was determined by PC6 Principal Component Analysis on the ASTER sensor.

-According to geological, petrographic, and geochemical evidence, there are two types of mineralization in Parwan-Panjshir AOI. The first type is related to the mineralization of hematite-magnetite iron small and large lenses with the crystalline limestone host-rock, which has existed in the region for a long time. The second type of mineralization in the study area is copper-iron and gold skarnization, which is younger due to the conformable of basalt-diabase units with carbonate units. This division has been confirmed by the lack of proper correlation between elements of two different types. In fact, although in the samples collected from iron-containing lenses, there is a high correlation between Fe and Ba, Sn, Ag, Mo, Nb, Sr, and W, there is a positive correlation between Cu and W. In both graphs there is no proper correlation between Fe and Cu.

-Due to the high volume of hematite iron with low FeO content and crystalline carbonate units, this reserve can be used in cement production.

-In order to find the copper-gold-skarn and iron lens deposits in the AOI, accurate mapping of the AOI should be prepared to plan a systematic sampling network. Furthermore, geophysical operations (for IP method for skarn zone and Magnetometer method for iron lenses to identify the magnetic part of the reserve) and subsurface drilling are recommended.

4.Acknowledge:

WE would like express our gratitude to OMG/OGC to provide us with modern equipment, facilities, and monetary supports for accomplishment of this study in Parwan-Panjshir AOI. Moreover, we would like to say thank you to all kind people who cooperate and help us in related to field survey, sample collection, sample preparation, so on.

Conflicts of Interest: The authors declare no conflict of interest.

References

1. Treloar, P.J. and C.N. Izatt, *Tectonics of the Himalayan collision between the Indian plate and the Afghan block: A synthesis.* Geological Society, London, Special Publications, 1993. 74(1): p. 69-87.
2. Molnar, P. and P. Tapponnier, *The collision between India and Eurasia.* Scientific American, 1977. 236(4): p. 30-41.
3. King, T.V., et al., *Hyperspectral remote sensing data maps minerals in Afghanistan.* Eos, Transactions American Geophysical Union, 2012. 93(34): p. 325-326.
4. Marjoribanks, R., *Geological methods in mineral exploration and mining*. 2010: Springer Science & Business Media.
5. Hunt, G.R., *Spectral signatures of particulate minerals in the visible and near infrared.* Geophysics, 1977. 42(3): p. 501-513.
6. Malistani, H., *Hajigak Iron Ore Deposit.* 2011.
7. Risen, J., *US identifies vast mineral riches in Afghanistan.* New York Times, 2010. 13.
8. Abdullah, S., V. Chmyriov, and V. Dronov, *Geology and mineral resources of Afghanistan*. 2008, British Geological Survey.
9. Azizi, M., H. Saibi, and G. Cooper, *Mineral and structural mapping of the Aynak-Logar Valley (eastern Afghanistan) from hyperspectral remote sensing data and aeromagnetic data.* Arabian Journal of Geosciences, 2015. 8(12): p. 10911-10918.
10. Abdullah, S., et al., *Mineral resources of Afghanistan: Kabul.* Afghanistan, Republic of Afghanistan Geological and Mineral Survey, 1977.

11. Will R. Stettner, N.E.K., Linda M. Masonic, and David A. Shields, *Geologic and Mineral Map (Modified from the 1975 Original Map Compilation by A.S. Shadchinev and others) and Hyperspectral Surface Material Maps of the Chorband, Salang, and Panjsher River Basins; Kapisa, Panjsher, Parwan, and Baghlan Provinces, Afghanistan.* 2020.
12. Khalaj, M., *Investigation and their Relationship of copper mineralizations of ChahMousa, Derakhshanieh and Qollehsoukhteh area with structural lineaments based on geochemistry ,alteration and fluid inclusion in the south of Damghan.* 2013.
13. Rowan, L.C., M.J. Kingston, and J.K. Crowley, *Spectral reflectance of carbonatites and related alkalic igneous rocks; selected samples from four North American localities.* Economic Geology, 1986. 81(4): p. 857-871.
14. Gabr, S.S., S.M. Hassan, and M.F. Sadek, *Prospecting for new gold-bearing alteration zones at El-Hoteib area, South Eastern Desert, Egypt, using remote sensing data analysis.* Ore Geology Reviews, 2015. 71: p. 1-13.
15. Ducart, D.F., et al., *Mapping iron oxides with Landsat-8/OLI and EO-1/Hyperion imagery from the Serra Norte iron deposits in the Carajás Mineral Province, Brazil.* Brazilian Journal of Geology, 2016. 46(3): p. 331-349.
16. Ranjbar, H., M. Honarmand, and Z. Moezifar, *Application of the Crosta technique for porphyry copper alteration mapping, using ETM+ data in the southern part of the Iranian volcanic sedimentary belt.* Journal of Asian Earth Sciences, 2004. 24(2): p. 237-243.
17. Peters, S.G., et al., *Preliminary Non-Fuel Mineral Resource Assessment of Afghanistan 2007.* US geological survey open-file report, 2007. 1214.
18. Dupuis, C. and G. Beaudoin, *Discriminant diagrams for iron oxide trace element fingerprinting of mineral deposit types.* Mineralium Deposita, 2011. 46(4): p. 319-335.